Applied Energy 377 (2025) 124499

Contents lists available at ScienceDirect

Applied Energy

journal homepage: www.elsevier.com/locate/apenergy

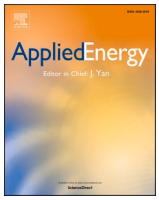

Investigating the efficiency of hybrid architectures for agricultural tractors using real-world farming data

Michele Mattetti [a,*], Gianvito Annesi [a], Francesco Pio Intrevado [a], Luigi Alberti [b]

[a] Department of Agricultural and Food Sciences, Alma Mater Studiorum, University of Bologna,Viale G. Fanin 50, 40127, Bologna, Italy
[b] Department of Industrial Engineering, University of Padova, Via G. Gradenigo, 6, Padova, Italy

HIGHLIGHTS

- A tractor was monitored for outlining its usage and its operational inefficiencies
- Two electrified architectures were investigated denoted as e-PTO and Plug-in P4.
- Both architectures was designed to optimise engine operating point.
- e-PTO permits to obtain a fuel saving up to 16 % on low demanding operations.
- Plug-in P4 achieves a CO_2 and cost savings of cost of 7.2 % and 9.5 %, respectively.

ARTICLE INFO

Keywords:
Fuel efficiency
Greenhouse gas emissions
Real-world data
Hybrid agricultural tractors

ABSTRACT

In 2020, the European Commission (EC) approved the European Green Deal, which is an ambitious package of measures that aim to transform Europe into a climate-neutral area. Agricultural machinery in Europe produces around 70 million tons of CO_2 emissions each year. Industry and researchers are currently investigating hybrid powertrains to significantly reduce CO_2 emissions. This paper aims to investigate two hybrid powertrain architectures and report the benefits to farmers of such solutions using real-world data. Real-world data were collected using a Controller Area Network (CAN-BUS) data logger on a row-crop tractor with an engine power of 158 kW. Engine and transmission operating parameters were recorded for more than two years of field use. Data were first classified into tasks and then a series of inefficiency indices were defined. The operational inefficiency of each task type was then identified. Two hybrid powertrain architectures were evaluated using load point shifting principles. These were electric power take-off (ePTO) and plug-in P4 architecture. The hybrid architecture with the greatest benefits was the plug-in P4 powertrain, which achieved cost and CO_2 savings of 7.2 % and 9.5 %, respectively. In the future, as the proportion of electricity from renewable sources increases, greater benefits could be achieved. On the other hand, the ePTO architecture permits to achieve a lower fuel saving, below than 2 %, but with a simpler technology.

1. Introduction

According to the European Environment Agency, agricultural machinery in Europe produces around 70 million tons of CO_2 emissions each year [1]. if no significant technological changes are implemented, this value is expected to rise in the future due to population growth and the consequent demands of a greater amount of food,. In 2020, the European Commission (EC) adopted the European Green Deal, which is an ambitious package of measures aiming to transform Europe into the first climate-neutral area. Previously, greenhouse gas (GHG) emissions from non-road mobile machinery were reduced through the successive tightening of emissions legislation (from Stage I in 1996 to Stage V in 2019). Major progress in further emissions reduction is not expected and therefore concerns were recently raised relating to fossil fuel use in agricultural machinery [2,3]. Academic researchers, industry, and policy-makers are compelled to search for novel solutions, with powertrain electrification considered a feasible solution to further reduce fuel consumption and GHG emissions [3,4], particularly as the proportion of electricity from renewable sources increases worldwide [5].

Agricultural tractors are used for tasks ranging from on-road transportation to heavy tillage operations, and their mechanical architectures

* Corresponding author.
E-mail address: michele.mattetti@unibo.it (M. Mattetti).

https://doi.org/10.1016/j.apenergy.2024.124499
Received 25 February 2024; Received in revised form 7 August 2024; Accepted 12 September 2024
Available online 21 September 2024

Nomenclature

$2WD$	two-wheel drive[−]
$4WD$	four-wheel drive[−]
C	daily cost saving[€]
c_e	cost of electricity[€ $kW^{-1}h^{-1}$]
c_{el}	cost of electricity[€ $kW^{-1}h^{-1}$]
c_f	cost of fuel[€ L^{-1}]
c_f	cost of electricity[€ $kW^{-1}h^{-1}$]
CD	charge depleting[−]
CO_2	carbon dioxide[−]
CS	charge sustaining[−]
D	differential[−]
EC	European Commission[−]
EG	electric generator[−]
EM	electric motor[−]
$ePTO$	electric PTO architecture[−]
E_e	energy delivered by the engine[kJ]
$\dot{f}_e$	measured engine fuel rate[Lh^{-1}]
$\dot{f}_{sc}$	specific fuel consumption[g $kW^{-1}h^{-1}$]
$\dot{f}_{sc,min}$.	minimum specific fuel consumption[g $kW^{-1}h^{-1}$]
$\dot{f}_{sc,opt}(P_e)$	optimal specific fuel consumption at power P_e[g $kW^{-1}h^{-1}$]
FD	front differential[−]
FR	final reducer[−]
FT	front tyre[−]
GHG	greenhouse gas[−]
$GNSS$	global navigation satellite system[−]
I	inefficiency index[−]
ICE	internal combustion engine[−]
k_p	fraction of engine power transmitted to the front axle[−]
LS	load shifting[−]
$mPTO$	mechanical PTO architecture[−]
M_e	measured engine torque[Nm]
$M_{e\%}$	actual engine - percentage torque[%]
m_{el}	emissions factor of electricity[−]
M_f	nominal friction - percentage torque[Nm]
m_f	emissions factor of fuel[kg L^{-1}]
M_{ice}	momentum delivered by the internal combustion engine [Nm]
$M^{PTO}_{ICE,max}$	maximum engine torque with PTO engaged[Nm]
$M_{ICE,max}$	maximum engine torque with PTO disengaged[Nm]
M_r	engine reference torque[Nm]
$NRMM$	Non-road mobile machinery[−]
$OECD$	Organisation for Economic Co-operation and Development [−]
P_d	power delivered by the battery[kW]
P_e	measured engine power[kW]
P^{PTO}_e	measured engine power when the PTO was engaged[kW]
$P_{ICE,lim}$	engine power where the specific fuel consumption is 1.2 times greater than $\dot{f}_{sc,min}$.[kW]
P_{ICE}	power delivered by the internal combustion engine in the ePTO and P4 architecture[kW]
$P_{ICE,opt}$	power delivered by the internal combustion engine when $\dot{f}_{sc,min}$.occurs[kW]
$P_{ICE,rated}$	engine rated power with PTO disengaged[kW]
$P^{PTO}_{ICE,rated}$	engine rated power with PTO engaged[kW]
P_r	power stored in the battery[kW]
$P_{req,PTO}$	requested power at the PTO shaft[kW]
PTO	power take-off[−]
PGN	parameter group number[−]
RD	rear differential[−]
RT	rear tyre[−]
S_{4WD}	transfer case selector switch[−]
S_{batt}	battery size[kWh]
SoC	state of charge[−]
SPN	suspect parameter numbers[−]
S_{4WD}	transfer case selector switch[−]
t_d	duration of a working day[s]
T_f	engine fuel temperature 1[°C]
V_t	tractor ground speed[km h^{-1}]
ρ_f	fuel density[kg m^{-3}]
η_{batt}	efficiency of the battery in the plug-in P4 architecture[−]
η_{ePTO}	efficiency of the generator/motor combination in the ePTO system[−]
η_g	effiency of the electric generator employed in the plug-in P4 architecture[−]
η_m	effiency of the electric motor employed in the plug-in P4 architecture[−]
η_{mPTO}	efficiency of engine-to-PTO transmission in the mPTO[−]
η_t	efficiency of the tractor transmission[−]
ω_e	measured engine speed[rpm]
ω_{ICE}	speed of internal combustion engine[rpm]
Δf_{ePTO}	potential fuel saving of ePTO architecture[L]
Δf_{P4}	potential fuel saving of plug-in P4 architecture[L]
ΔM_{CO_2}	daily CO_2 saving of plug-in P4 architecture[kg]
Δt	sampling period[s]

have not changed significantly in the past 60 years. In particular, mechanical power is delivered by an internal combustion engine (ICE) and transmitted to the wheels, power take-off (PTO), and hydraulic outlets. This architecture has several limitations due to varying field loads, which can lead to suboptimal operating conditions. These limitations include: *i)* mechanically driven accessories; *ii)* lack of idling stop technology; and *iii)* ICE operating outside of its optimal power range. As a part of the Green SEED project, technical limitations *i)* and *ii)* were addressed in detail through other studies by the authors [6–8]; therefore, this study was focused on investigating technical limitation *iii)*.

ICEs can achieve optimal specific fuel consumption only when they operate within a certain power range; otherwise, their efficiency reduces considerably [9]. So, ICEs can be efficient if they are appropriately sized, and the car industry has been adopting downsizing principles to increase fuel efficiency [10]. Therefore, appropriate engine sizing is a crucial step in achieving high operational efficiency; however, this can be challenging to achieve for agricultural tractors. This is because agricultural tractors are used for low energy demanding operations (i.e. idling and headland turns) approximately 33 % of the time [11], whilst for the remainder of the time, they operate at high but varying engine loads due to changing operating and environmental conditions. Suboptimal specific fuel consumption occurs also during PTO operations since by the PTO, which must operate at its nominal speeds (i.e. 540 rpm and 1000 rpm); the PTO is mechanically coupled to the engine with a gearbox, leading to nominal PTO speeds at certain engine speeds as a function of the PTO operating mode: standard or economy. Generally, in standard and economy PTO modes, the nominal speeds occur when the engine delivers peaks in power and torque, respectively. Thus, when the power delivered by the ICE is significantly lower than the maximum power that the ICE can deliver at a particular engine speed, unnecessary ICE overspeed may occur, leading to suboptimal operating conditions. To avoid such overspeed, several manufacturers have released hydraulic-driven implements, and despite the energy conversion, greater fuel efficiency was observed in low demand operations (e.g. planting and spreading)

than the mechanical alternatives [12]. Under these conditions, solutions are necessary to shift unfavourable engine operating points to more favourable points to achieve high operational efficiency in ICEs.

These limits could also be overcome using appropriate electrification architecture, and interest in this subject amongst researchers has increased significantly in recent years [3,4,9,13–16]. In addition, the industry of agricultural machinery is also actively investigating this subject, as demonstrated recently through the presentation of prototypes at leading fairs (i.e. Landini REX4 Electra, Antonio Carraro SRX Hybrid, New Holland T4 Electric Power, Carraro Agricube Hybrid, and John Deere 8R 410 eAutoPowr). These prototypes had adopted different architectures, demonstrating that there is no established practice in the industry. This is because the identification of appropriate hybrid architectures is challenging due to the particular uses of agricultural tractors, the multiple power paths, and the multiple degrees of freedom (i.e. multiple architectures, sizing, control solutions, etc.).

Several studies have reported that the lack of a reference cycle is a limiting factor when designing hybrid powertrains for agricultural tractors [3], and the authors of this study have investigated this aspect by proposing a methodology for developing a synthesis of a prolonged field usage [17]. Independent agencies (e.g. Environmental Protection Agency) have investigated the potential benefits of off-cycle technologies, which are measures that give credit for vehicle efficiency improvements beyond homologation processes [18]. Off-cycle technology should be investigated using real-world data collected from tractors in use by farmers. Given the large number of sensors embedded into Controller Area Network (CAN-BUS) systems, data-driven approaches are now possible, and they should be adopted to guide the design of novel hybrid architectures leading to fuel-saving in real-world farming. Considering this scenario, this study reports a novel data-driven methodology to guide the design of tractor architectures and evaluate potential fuel savings in real-world farming that are equivalent to farmer's point-of-view fuel savings. The paper describes the collection of real-world data, which was used to characterise field tasks in terms of operational efficiency, and using a simplified approach, estimates the fuel potential savings achievable using two hybrid architectures.

2. Materials and methods

2.1. Data collection

This study used a New Holland T7 tractor (CNH Industrial N.V., Amsterdam, Netherlands) with specifications as reported in Table 1. This model was selected because tractors of this class contain an array of sensors that enable comprehensive monitoring of the embedded subsystems (i.e. engine, gearbox, PTO, and three-point linkage).

The tractor was in use between June 2018 and January 2021 at the Agricultural Farm of the University of Bologna, in Granarolo municipality, Italy. The tractor was mainly used for transportation and primary and secondary tillage tasks and was routinely driven by professional drivers.

A standalone CAN-BUS data logger optimised by CNH Industrial was installed on the tractor. The data logger was set up to automatically record all CAN-BUS messages whenever the tractor engine was turned on so that the recording process did not interfere with any farming activities. In particular, the CAN-BUS data logger was equipped with two separate CAN-BUS channels compatible with the standards SAE J1939–14 [19] and SAE J1939–15 [20]. Only signals with the following suspect parameter numbers (SPNs) and parameter group numbers (PGNs) [21,22] were used in the analysis:

- SPN 544 and PGN 65251: "*engine reference torque*", which reports the maximum torque the engine can deliver, denoted as M_r and sampled every 5 s.
- SPN 513 and PGN 61444: "*actual engine - percent torque*", which reports the torque as a percentage of M_r, denoted as $M_{e\%}$ and sampled every 20 ms.
- SPN 513 and PGN 5398: "*nominal friction-percent torque*", which reports the frictional and thermodynamic loss of the engine itself, pumping torque loss, and the losses of fuel, oil, and cooling pumps as a percentage of M_r, denoted as M_f and sampled every 250 ms.
- SPN 190 and PGN 61444: "*engine speed*", which reports the revolution speed of the engine crankshaft, denoted as ω_e and sampled every 250 ms.
- SPN 1883 and PGN 65090: "*rear PTO output shaft speed*", which reports the speed of the rear PTO and sampled every 100 ms.
- SPN 1882 and PGN 65090: "*front PTO output shaft speed*", which reports the speed of the front PTO and sampled every 100 ms.
- SPN 1873 and PGN 65093: "*rear hitch position*", which reports the position of the rear three-point linkage, expressed as a percentage of full travel and sampled every 100 ms.
- SPN 183 and PGN 65266 "*engine fuel rate*", which reports the fuel consumed by the engine per unit of time, denoted as $\dot{f}_e$ and sampled every 100 ms.
- SPN 174 and PGN 65262 "*engine fuel temperature 1*", which reports the temperature of the fuel, denoted as T_f and sampled every 1 s.
- SPN 2796 and PGN 64980 "*transfer case selector switch*", which reports the mode of the transmission and is denoted as S_{4WD} and sampled every 10 s. This signal was 1 when the tractor operated in four-wheel drive (4WD) mode and 0 when in two-wheel drive (2WD) mode.

In addition, a global navigation satellite system (GNSS) receiver with an update rate of 10 Hz and no differential correction (IPEspeed, IPETRONIK GmbH, Baden-Baden, Germany) was installed in the tractor to monitor its position and ground speed (V_t).

2.2. Data analysis

All portions of the recorded signals acquired when the tractor position was not logged were excluded from the analysis. Moreover, all days

Table 1
Main specifications of the tractor used in this study. The reported data were sourced from the manufacturer's brochure. The values 540 and 1000 represent the standard PTO mode with a nominal speed of 540 rpm and 1000 rpm, respectively. The values 540E and 1000E represent economy PTO mode with a nominal speed of 540 rpm and 1000 rpm, respectively.

Engine displacement	$[cm^3]$	*6728*
Number of cylinders	[–]	*6*
Engine tier	[–]	*4 A*
Engine rated power with PTO disengaged ($P_{ICE,rated}$)	[*kW@rpm*]	*158@2200*
Engine rated power with PTO engaged ($P^{PTO}_{ICE,rated}$)	[*kW@rpm*]	*181@2200*
Maximum engine torque with PTO engaged ($M_{ICE,max}$)	[*Nm@rpm*]	*995@1500*
Maximum engine torque with PTO engaged ($M^{PTO}_{ICE,max}$)	[*Nm@rpm*]	*1120@1500*
Transmission	[–]	*Full powershift with 19 forward and 6 rearward gears*
Engine speed at PTO 540/540E/1000/1000E speed	[*rpm*]	*1931/1598/1912/1583*

with less than 30 min of recorded data were removed from the analysis as they may have related to ancillary activities such as servicing. This filtering simplified the subsequent data analysis.

Signals were interpolated with a sampling period (Δt) of 0.1 s using a cubic spline for a consistent sampling rate. From the recorded data, the measured engine torque (M_e), power (P_e), specific fuel consumption ($\dot{f}_{sc}$), and energy delivered by the engine (E_e) were calculated using Eq. 1, Eq. 2, Eq. 3, and Eq. 4, respectively:

$$\mathrm{M_e} = \mathrm{M_r}\frac{\mathrm{M_{e\%}} - \mathrm{M_f}}{100} \tag{1}$$

$$\mathrm{P_e} = \mathrm{M_e}\omega_\mathrm{e}\frac{2\pi}{60} \tag{2}$$

$$\dot{\mathrm{f}}_{\mathrm{sc}} = \frac{\dot{\mathrm{f}}_\mathrm{e}\rho_\mathrm{f}}{\mathrm{P_e}} \tag{3}$$

$$\mathrm{E_e} = \int \mathrm{P_e dt} \tag{4}$$

where ρ_f is the density of fuel corrected by the function of T_f using data reported by Esteban et al. [21]. The $\dot{f}_{sc}$ signal was filtered through a third order median filter to avoid anomalies occurring on abrupt changes in engine loads, which could lead to unrealistically high values of $\dot{f}_{sc}$. Values of $\dot{f}_{sc}$ obtained in this way differed less than 5 % from those reported in the Organisation for Economic Co-operation and Development (OECD) report on the tractor model used in this study [22]. This enabled a sufficiently reliable brake-specific fuel consumption map to be obtained for the tractor. For each power level, the optimal specific fuel consumption ($\dot{f}_{sc,opt}(P_e)$) was the point of minimum specific fuel consumption (Fig. 1).

This enabled the calculation of an inefficiency index (I) using Eq. 5.

$$\mathrm{I(t)} = \frac{\dot{\mathrm{f}}_{\mathrm{sc}}(\mathrm{t}) - \dot{\mathrm{f}}_{\mathrm{sc,opt}}(\mathrm{P_e(t)})}{\dot{\mathrm{f}}_{\mathrm{sc,opt}}(\mathrm{P_e(t)})}100 \tag{5}$$

All of the recorded and calculated signals were classified according to the types of agricultural activities performed using the classification scheme proposed by Mattetti et al. [23]. According to this approach, the portions of data were classified into one of the following work states: idling, pass with PTO, pass without PTO, headland turn, moving, and unclassified (i.e. data that could not be classified under any of the other states) (Fig. 2). Moreover, data were further classified by traction mode (i.e. 2WD and 4WD modes) in function of S_{4WD}. This enabled mapping of the operational efficiency of the tractor in different work states.

2.3. Evaluation of the fuel savings of selected hybrid solutions

Based on the literature review and analysis of recorded data, two hybrid architectures – electric PTO (ePTO) and plug-in P4-architecture – were selected. For each hybrid architecture, the subsequent fuel savings were determined.

In Fig. 3, the mechanical PTO architecture (mPTO) and ePTO architecture are compared. Of note, in the ePTO, the PTO was run by the ICE through an electric generator/motor transmission. Thus, the PTO could be controlled by a type of continuously variable transmission, permitting the PTO to run at the requested nominal speed independently of the engine speed. The electric generator (EG) and electric motor (EM) were sized to provide $\mathrm{P^{PTO}_{ICE,rated}}$ as their nominal powers.

The ePTO architecture had to deliver the same requested power at the PTO shaft ($P_{req,PTO}$) which was calculated using Eq. 6.

$$\mathrm{P_{req,PTO}} = \mathrm{P_e^{PTO}}\eta_{\mathrm{mPTO}} \tag{6}$$

where P_e^{PTO} is the measured engine power when the PTO is engaged and η_{mPTO} is the efficiency of the engine-to-PTO transmission in the mPTO system, which was set at 0.96. This value assumed due to the fact that there are two gear meshes in the mechanical engine-to-PTO transmission of commercial tractors and that for each gear mesh, a constant efficiency of 0.98 was achieved as identified by Mattetti et al. [24]. Eq. 6 assumes that the entire engine power is transmitted to the PTO, providing a conservative estimate of the fuel savings. Using $P_{req,PTO}$, the power the ICE in the ePTO architecture (P_{ICE}) must deliver was calculated using Eq. 7.

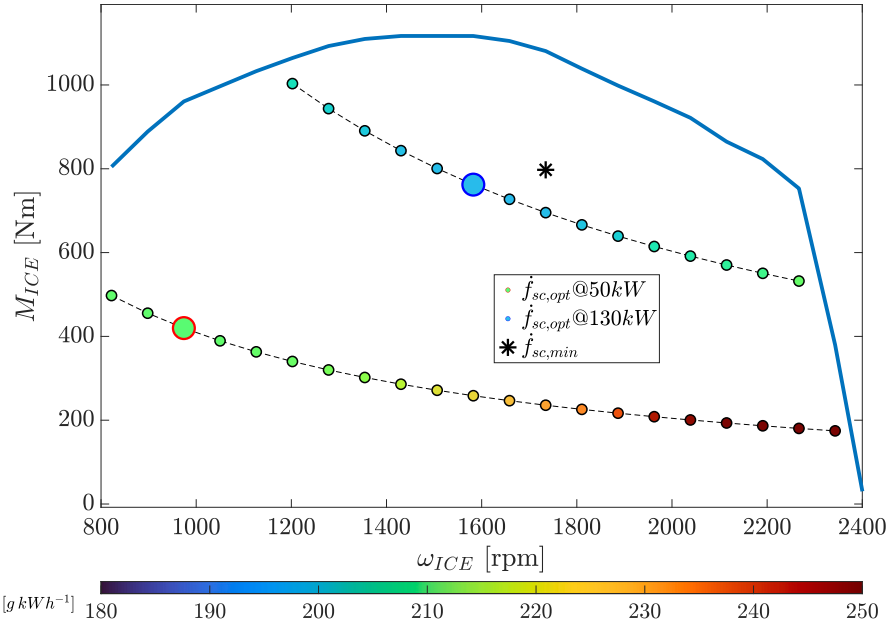

Fig. 1. Definition of the optimal operating points for two isopower curves. In contrast to the other operating points, these points are denoted by red and blue outline colours. The series of points shows the specific fuel consumption ($\dot{\mathrm{f}}_{\mathrm{sc}}$) along two isopower curves. $\mathrm{M_{ICE}}$ is the engine torque, ω_{ICE} is the engine speed, $\dot{\mathrm{f}}_{\mathrm{sc,opt}}$ is the minimum specific fuel at a certain engine power, and $\dot{\mathrm{f}}_{sc,min}$ is the global minimum specific fuel consumption. (For interpretation of the references to colour in this figure legend, the reader is referred to the web version of this article.)

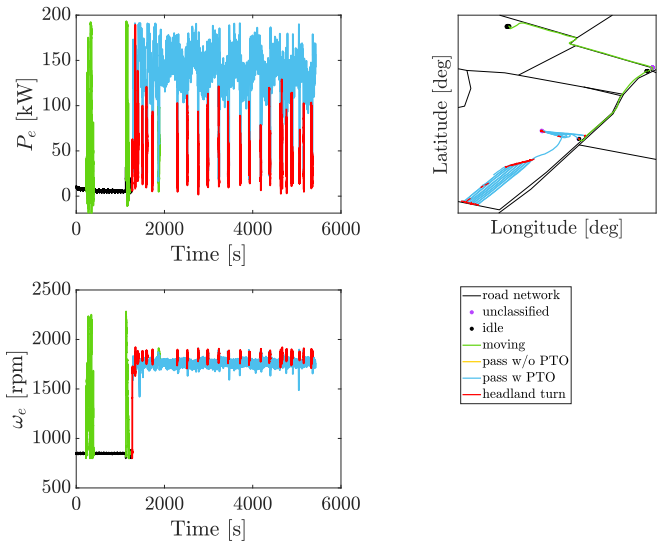

Fig. 2. Sample of the classification of the tractor work state: temporal trend of the measured engine power (P_e) (top left) and measured engine speed (ω_e) (bottom left) and tractor trajectory (top right).

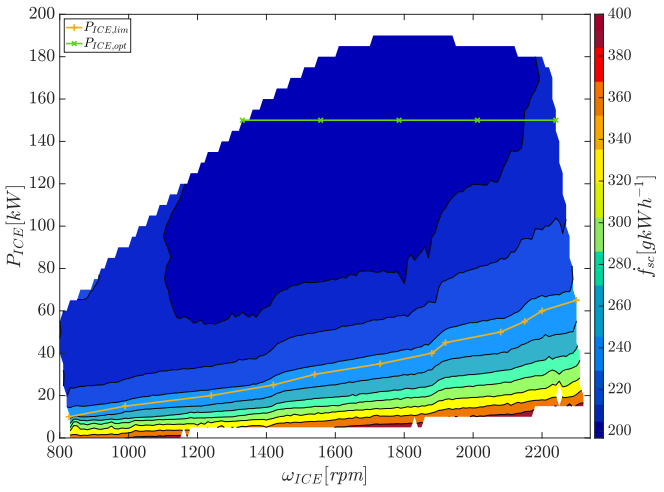

Fig. 5. Brake-specific fuel consumption map of the internal combustion engine (ICE) showing the isopower lines marking the areas of operational demand. ω_{ICE} is ICE speed, P_{ICE} is the power delivered by the ICE, $\dot{f}_{sc}$ is the specific fuel consumption, $P_{ICE,lim}$ is the P_{ICE} when $\dot{f}_{sc}$ is 1.2 times greater than the mininum specific fuel consumption, and $P_{ICE,opt}$ is the power delivered by the ICE when the minimun specific fuel consumption occurs.

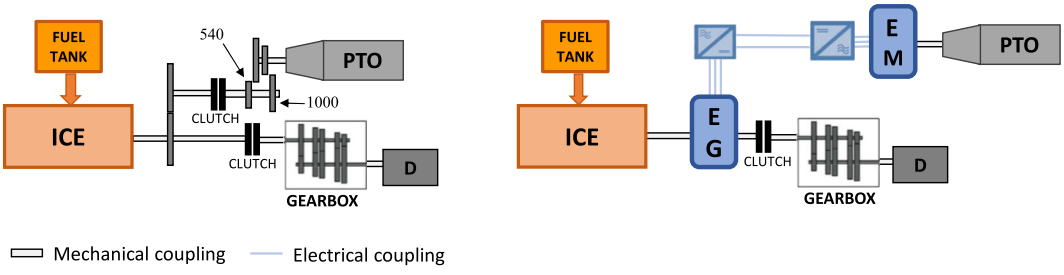

Fig. 3. Schematic descriptions of the mPTO (left) and ePTO (right) systems, with reference to the internal combustion engine (ICE), power take-off (PTO), electric generator (EG), electric motor (EM), and differential (D).

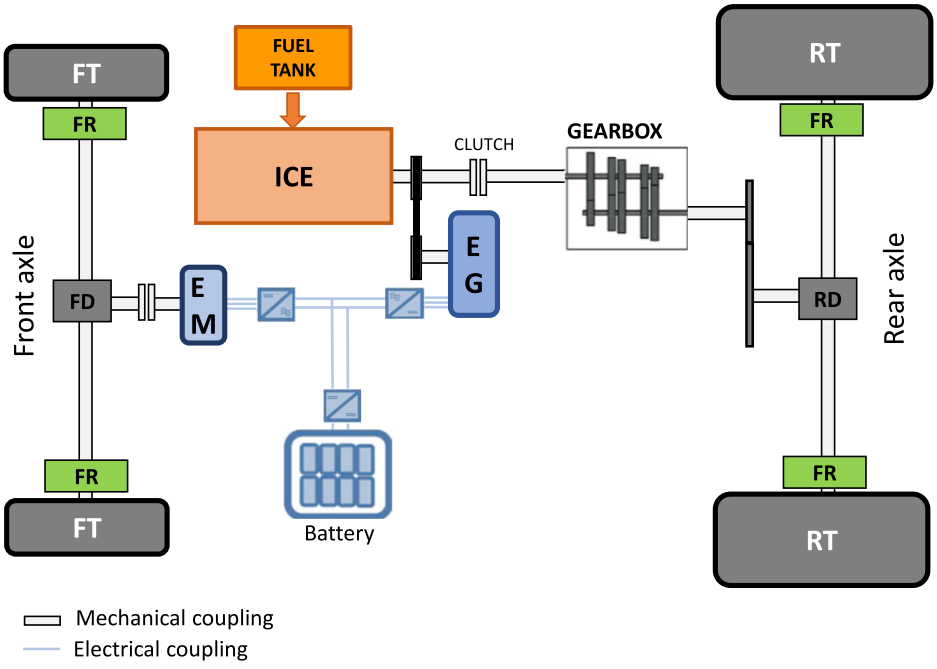

Fig. 4. Schematic description of the plug-in P4 architecture with reference to the internal combustion engine (ICE), electric motor (EM), electric generator (EG), front differential (FD), rear differential (RD), final reducer (FR), front tyres (FT), and rear tyres (RT).

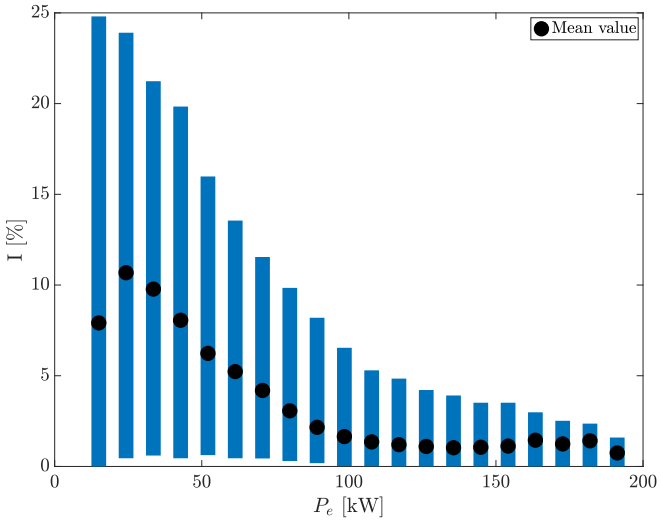

Fig. 7. 10th and 90th percentiles of the inefficiency index (I) with respect to the measured engine power (P_e).

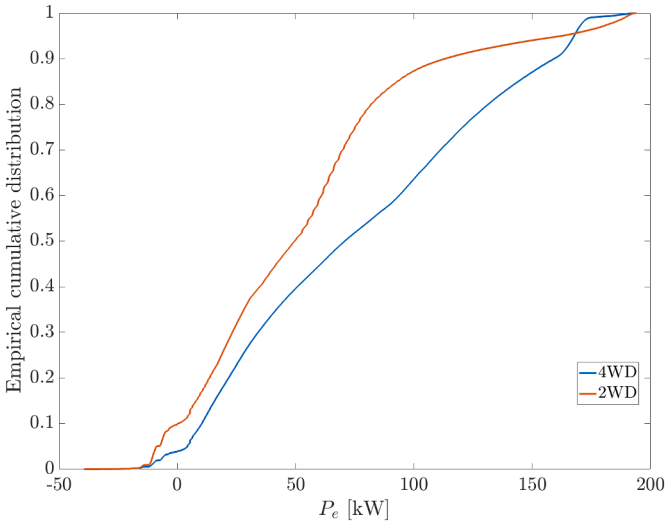

Fig. 9. Empirical cumulative distribution of measured engine power (P_e). Negative power occurred when the engine was spun by the wheels.

$$P_{ICE} = \frac{P_{req,PTO}}{\eta_{ePTO}} \tag{7}$$

where η_{ePTO} is the total efficiency of the generator/motor combination in the ePTO system. In this study, η_{ePTO} was set at 0.92 following Alberti et al. [25]. With the ePTO system, the engine operating point could be optimised by shifting it along the isopower curve to achieve the minimum $\dot{f}_{sc}$ for P_{ICE} $\dot{f}_{sc,opt}(P_{ICE})$ (Fig. 1). Using this approach, the potential fuel saving of the ePTO architecture with respect to mPTO (Δf_{ePTO}) was calculated using Eq. 8.

$$\Delta f_{ePTO} = \left(\dot{f}_{sc}(P_e)P_e^{PTO} - \dot{f}_{sc,opt}(P_{ICE})P_{ICE}\right) \Big/ \rho_f \tag{8}$$

The plug-in P4 architecture investigated in this study is summarised in Fig. 4. In particular, the front axle was disconnected from the propeller shaft and driven through an electric transmission (comprising a combination of electric generator and motor). A lithium-ion battery was installed to enable engine operating point optimisation in certain operating conditions, as described later in this paper. The ICE of the tractor was the same as that used by the tractor under investigation (Table 1).

The electric motor in the front axle was sized to deliver only a certain proportion (k_p) of the rated power delivered by the ICE through the through transmission (i.e. gearbox, differentials, and final drive) ($P_{ICE,rated}$). In particular, given that the power delivered by the front axle is proportional to the fraction of the mass on the front axle with respect to the total mass of the tractor [26], as 40 % of tractor mass was on the front wheels is expected in typical field operations, a k_p of 0.4 was chosen. The operating conditions of the tractor were classified as either low, medium, or high demand based on the rules described in Table 2.

$P_{ICE,opt}$ is the engine power at the point of minimum specific fuel consumption ($\dot{f}_{sc,min}$), corresponding to 150 kW (Fig. 5), whilst $P_{ICE,lim}$ occurred when $\dot{f}_{sc}$ was 1.2 times greater than $\dot{f}_{sc,min}$.

Two battery states were defined based on the state of charge (*SoC*) of the battery (Table 3).

For the low classification, the upper limit of the *SoC* was chosen to limit the depth of discharge of the battery and achieve an adequate battery cycle life in accordance with Markel and Simpson [27]. The ICE

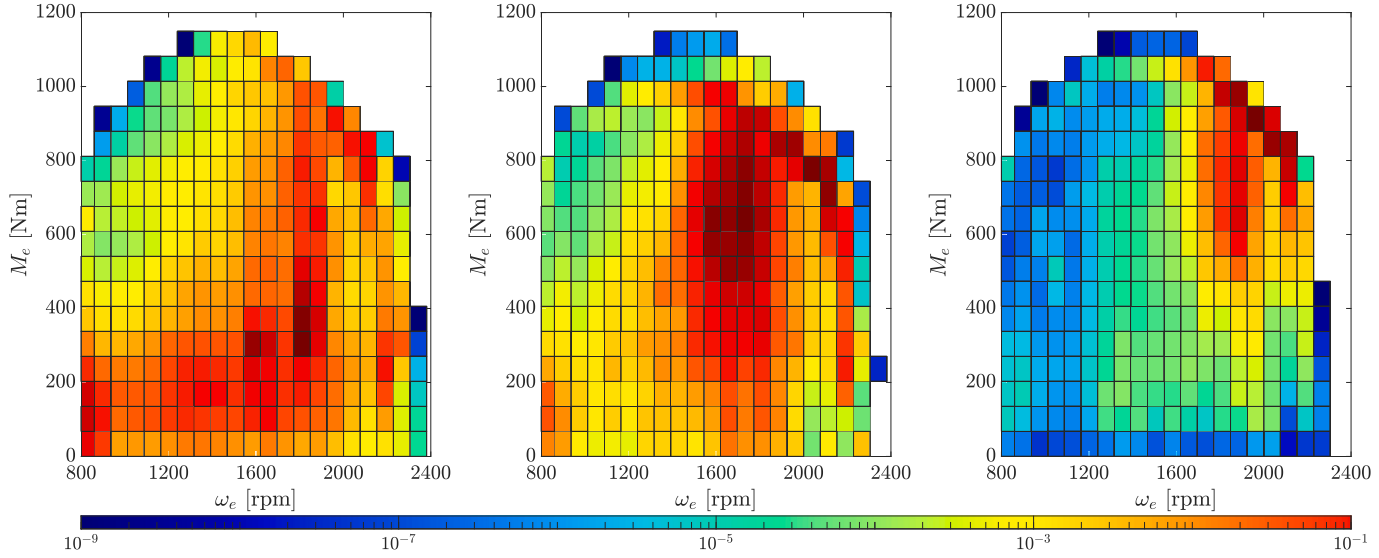

Fig. 8. Relative frequency distribution maps of engine torque (M_e) and engine speed (ω_e) for moving states (on the left), pass without PTO (on the centre), pass with PTO (on the right).

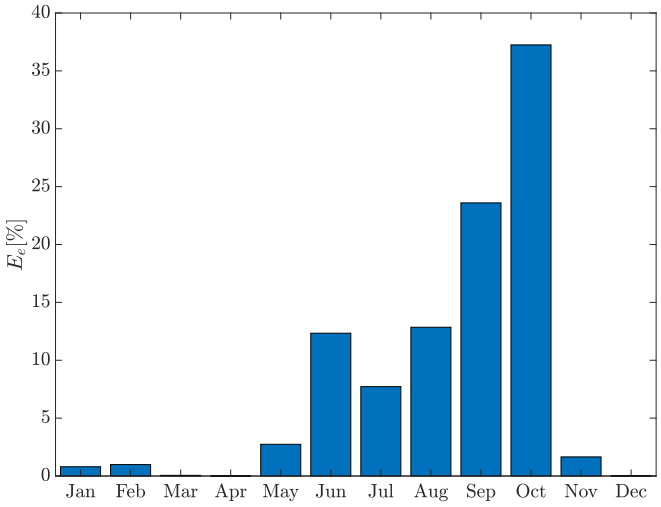

Fig. 10. Monthly use of energy delivered by the engine (E_e). E_e is reported as a percentage of the annual value of E_e.

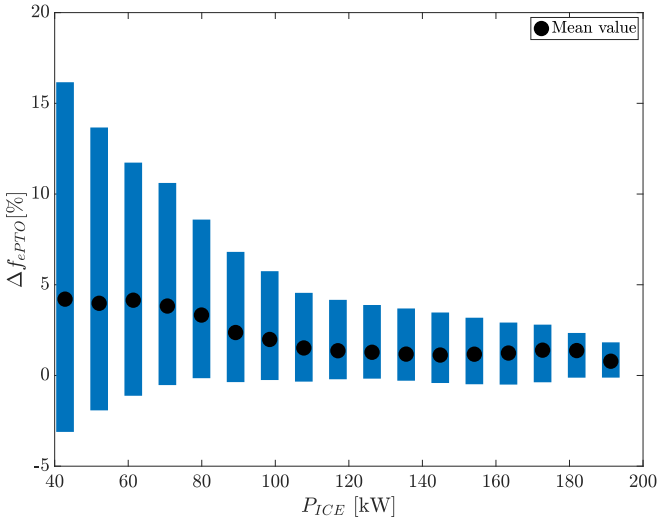

Fig. 11. Range of potential fuel savings of ePTO architecture (Δf_{ePTO}) with respect to the power delivered by the ICE (P_{ICE}), which are shown in binned intervals.

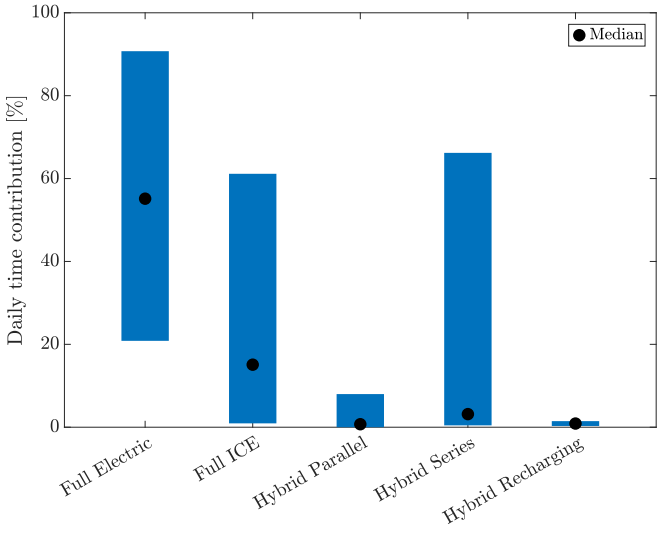

Fig. 12. Daily time contribution of each operating mode for a battery capacity of 44 kWh.

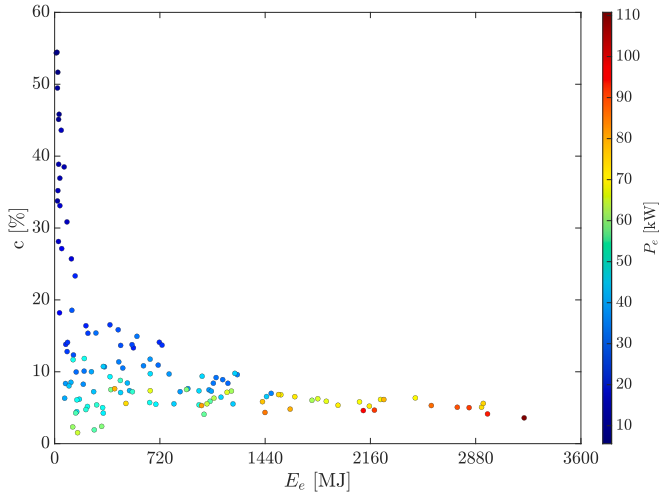

Fig. 13. Daily cost saving (C) with respect to the daily energy generated by the engine (E_e) and measured engine power (P_e). Each point corresponds to a single day.

Fig. 14. Temporal trend in the cost savings of the plug-in P4 architecture together with the historical trends in energy cost increases with respect to costs in 2015.

Table 2
Classification of operating demand.

Operating demand	*Rule*
Low	$P_e \leq P_{ICE,lim}$
Medium	$P_{ICE,lim} < P_e \leq P_{ICE,opt}$
High	$P_e \geq P_{ICE,opt}$

Table 3
Battery states as a function of battery SoC.

SoC classification	*Rule*
Full	$0.3 < SoC \leq 1$
Low	$SoC \leq 0.3$

may have been off or operating in three modes, namely charge sustaining (CS), charge depleting (CD), and load shifting (LS). For each operating mode, P_{ICE} is reported in Table 4. In CS mode, the ICE operated in a load-following mode, and in CD mode, the wheel power was delivered from the ICE and the battery, whilst in LS mode, the ICE was forced to operate at the point where $\dot{f}_{ICE,opt}$ occurs, delivering $P_{ICE,opt}$.

Table 4
ICE operating modes.

ICE operating mode	$S_{4WD} = 0$	$S_{4WD} = 1$
Off	*0*	*0*
CS	$P_{ICE} = P_e$	$P_{ICE} = P_e\left(1 - k_p + k_p\frac{\eta_t}{\eta_g\eta_m}\right)$
CD	–	$P_{ICE} = P_{ICE,opt}$
LS	$P_{ICE} = P_{ICE,opt}$	$P_{ICE} = P_{ICE,opt}$

In Table 4, η_t, η_g, and η_m are the efficiency of the mechanical transmission (i.e. gearbox, differential, and final reducer), electric generator, and electric motors, respectively. In this study, η_t was set at 0.81 (there were six gear meshes in the gearbox and a differential and final reducer on each axle, with an assumed constant efficiency of 0.98 for each gear mesh [24], 0.95 for the differential reducer, and 0.97 for the final reducer [28]), whilst η_g and η_m were set at 0.96 and 0.95, respectively, in accordance with Alberti and Troncon [25]. In CS mode, when S_{4WD} was equal to 1, part of the power was delivered through the electric transmission of the front axle, which may have had a different efficiency to that of the mechanical transmission of the conventional tractor. To maintain the same wheel power, the fraction of ICE power transmitted to the front axle was adjusted by the factor $\eta_t\,\eta_g^{-1}\,\eta_m^{-1}$. The rules in Table 4 were used to set an appropriate state strategy, which was used to make the tractor operate according to a series of heuristic rules defined on the basis of the analysis of real-world data (Table 5).

According to Table 5, the tractor could operate in three operating modes, namely full ICE, hybrid, and full electric. In full ICE mode, traction was only at the rear wheels, whilst in full-electric mode, traction was forced to the front wheels. Except for low demand operations and when the battery was at a full state (Table 3), the setting for the front assistance chosen by the driver was maintained in the plug-in P4 architecture. Hybrid mode could be divided into three categories, namely series, parallel, and recharging. The first two modes occurred only in 4WD while series occurs when no power from the battery was delivered. Hybrid recharging mode was dedicated to recharging the battery. The data recorded and described in Section 2.1 was grouped by day and starting with the ω_e, and P_e signals, the power flows in the powertrain were simulated using a dedicated model, enabling the calculation of P_{ICE}, ICE fuel rate ($\dot{f}_{ICE}$), and battery *SoC*. For this simulation, it was assumed that the battery was fully charged overnight using energy from the grid, leading to an initial *SoC* each day equal to 1. The actual *SoC* ($SoC(t)$) was calculated using Eq. 9 from the *SoC* of the previous time step ($SoC(t-\Delta t)$).

$$\mathrm{SoC(t)} = \mathrm{SoC(t-\Delta t)} - \frac{\mathrm{P_d - P_r}}{\mathrm{S_{batt}}}\Delta \mathrm{t} \tag{9}$$

where P_d is the power delivered by the battery, P_r is the power recharged in the battery, S_{batt} is the energy capacity of the battery, and Δt is the time step of the simulation, which was set as 0.1 s. In ICE operating mode, P_d and P_r were calculated as described in Table 6, enabling calculation of the temporal trend of *SoC*, P_{ICE}, and $\dot{f}_{ICE}$ (Fig. 6).

where η_{batt} is the efficiency of the battery, which was set at 0.88 in this study. The fuel saving (Δf_{P4}) was calculated using Eq. 10, whilst the daily consumption of electrical energy from the grid (E_{el}) was calculated using Eq. 11.

$$\Delta \mathrm{f_{P4}} = \int_0^{\mathrm{t_d}} \left(\dot{\mathrm{f}}_{\mathrm{e}} - \dot{\mathrm{f}}_{\mathrm{ICE}}\right) \mathrm{dt} \tag{10}$$

$$\mathrm{E_{el}} = (1 - \mathrm{SoC(t_d)})\mathrm{S_{batt}} \tag{11}$$

where t_d is the duration of a working day and $SoC(t_d)$ is the final SoC of the day. S_{batt} was set to be similar in volume to the largest installable ballast that could be accommodated on the tractor without impairing operator visibility. Therefore, the volume of ballast was set at 0.16 m^3, whilst the maximum battery capacity was set at 44 kWh based on an energy density of 270 kWh m^3 for lithium-ion batteries [29]. The daily cost saving (C) was calculated using Eq. 12.

$$\mathrm{C} = \mathrm{c_f}\Delta \mathrm{f_{P4}} - \mathrm{c_e}\mathrm{E_{el}} \tag{12}$$

where C_{el} and c_f are the cost of electricity and fuel, respectively. For this study, c_e was assumed to be 0.16 € kWh^{-1} and c_f was assumed to be 0.9 € L^{-1} respectively, which represent the mean costs in Italy for the last 10 years [30,31]. Average values were used due to the variability in energy costs in the last few years. Moreover, CO_2 savings (ΔM_{CO_2}) were calculated using Eq. 13.

$$\Delta \mathrm{M_{CO_2}} = \Delta \mathrm{f_{P4}}\mathrm{m_f} - \mathrm{E_{el}}\mathrm{m_{el}} \tag{13}$$

where $\mathrm{m_f}$ and m_{el} are the CO_2 emission factors for the fuel and electricity production, respectively. The former was set at 2.624 kg L^{-1} [32], whilst the latter was set at 0.284 kg kWh^{-1} [33].

Table 5
List of operating modes of the plug-in P4 architecture.

State ID	*Operating classification*	*SoC level*	*ICE operating mode*	S_{4WD}
Full electric	*Low*	*Full*	*Off*	*Any*
Hybrid series	*Medium*	*Full / Low*	*CS*	*1*
	High	*Low*	*CS*	*1*
Hybrid parallel	*High*	*Full*	*CD*	*1*
Hybrid recharging	*Low*	*Low*	*LS*	*Any*
Full ICE	*Medium / High*	*Full / Low*	*CS*	*0*

Table 6
Formulas used to calculate the power delivered by the battery ($\mathrm{P_d}$) and the power stored in the battery ($\mathrm{P_r}$,) for each ICE operating mode.

ICE operating mode	P_d	P_r
Off	$\frac{P_e\eta_t}{\eta_m\eta_{batt}}$	0
CS	0	0
CD	$(P_e - P_{ICE,opt})\frac{\eta_t}{\eta_m\eta_{batt}}$	0
LS	0	$S_{4WD} = 0 \rightarrow (P_{ICE,opt} - P_e)\eta_g\eta_{batt} S_{4WD} = 1 \rightarrow \left(P_{ICE,opt} - P_e\left(1 - k_p + k_p\frac{\eta_t}{\eta_g\eta_m}\right)\right)\eta_g\eta_{batt}$

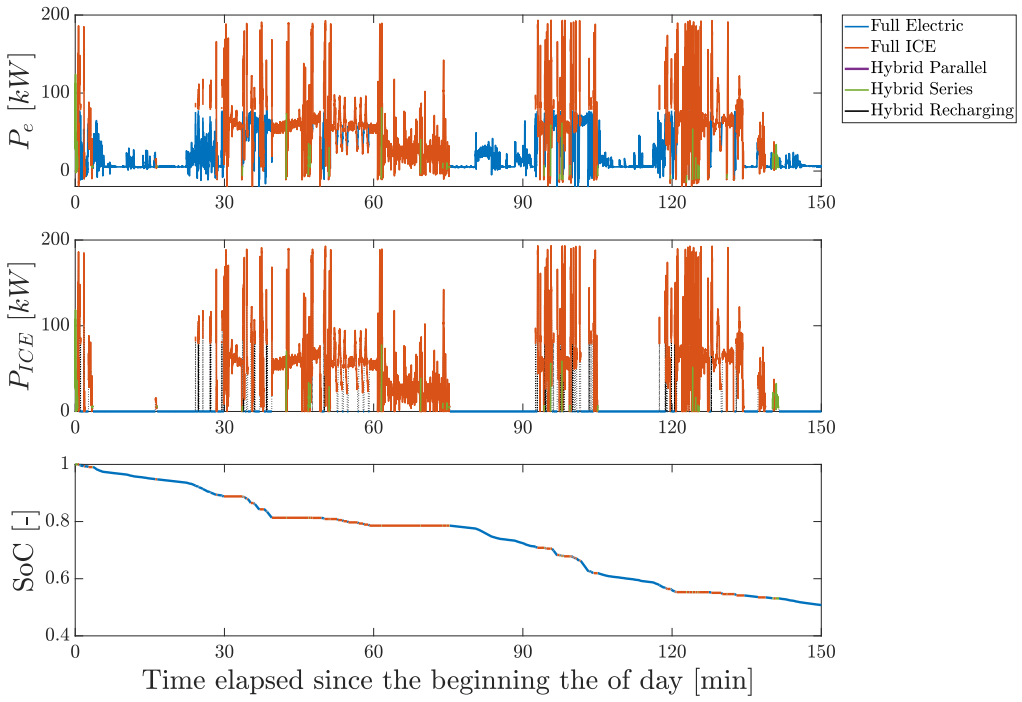

Fig. 6. Temporal trends in measured engine power (P_e) (top), power of the ICE in the plug-in P4 architecture (P_{ICE}) (middle), and the state of charge (SoC) for the plug-in P4 architecture (bottom).

3. Results and discussion

3.1. Real-world data analysis

The first part of this section summarises the results of the tractor's usage, whilst the second part reports the potential fuel savings for each of the hybrid architectures. During the monitoring period, the tractor was in operation for 177 days, accumulating 793 h, and consumed 13,465 L of fuel. Table 7 reports the proportion of time and fuel consumption for each work state, together with mean values for ω_e, P_e, $\dot{f}_{sc}$, and I.

The moving and passes states together accounted for approximately 68 % of the tractor usage. These results are aligned with those reported in other studies by the authors [11,23]. However, the passes states consumed the largest amount of fuel (56 %) because in these states the engine was required to deliver the greatest power. Indeed, the mean value of P_e for the passes states was up to 76 % greater than for the moving state. The P_e for the pass with PTO state was 56 % greater than that of the pass without PTO state. This was probably due to the specific use of the tractor but may also have been because the field operations were usually carried out at slow speed and the power was transmitted only through the transmission. In these conditions, the engine cannot deliver its maximum power due to the traction limit imposed by wheel-soil friction [34]. Moreover, the engine control unit commanded the engine to increase the maximum power by 23 kW when the PTO was engaged compared to when it was not engaged (Table 1). This increased the likelihood of a greater P_e with the PTO engaged compared to when the PTO was disengaged.

The mean value of ω_e on the passes states when the PTO was engaged was approximately that required to permit to the PTO shaft to rotate at the nominal speed, especially in standard mode (i.e. 540 rpm or 1000 rpm) (Table 1). However, ω_e on the passes states when the PTO was not engaged was between the engine speeds where maximum torque and power occur. This is the typical range recommended by manufacturers to maximise the benefits of engine stability and, according to the authors' experience, this recommendation is often followed by farmers.

The values of $\dot{f}_{sc}$ and I are negatively correlated with P_e (the Pearson correlation coefficient is −0.77 for the former and − 0.79 for the latter) because the most inefficient operating points for engines occur when the engine load and the delivered power are low. As expected, the highest mean value of $\dot{f}_{sc}$ was observed for the idling state, whilst the lowest was observed for the pass with PTO state, which was only 1.2 % lower than that of the pass without PTO state. The values for I ranged from 3.2 % to 6.3 %, indicating that there were opportunities for improvement in terms of fuel efficiency. Moreover, I increased with a decrease in P_e as is clearly shown in Fig. 7. In particular, I ranged from 0 (when the engine operated at the most efficient point for a certain level of P_e) up to a finite value depending on the maximum value of $\dot{f}_{sc}$ along the isopower curve. The lower the P_e, the greater the maximum value of $\dot{f}_{sc}$ on the isopower curve, and consequently, the range of I. Moreover, the lower the P_e, the greater the amount of engine operating points, and therefore the greater the likelihood that the engine operated at inefficient engine operating points, meaning that the was greater potential improvement possible through engine operating point optimisation.

In Fig. 8, the relative frequency distribution maps of the engine operating points for the three major work states are shown. Whilst idling is a frequent operating state for agricultural tractors, the distribution map for the idling state was not reported because it was concentrated in a small region. As the figure demonstrates, operating points were spread under the engine torque curve, particularly for the moving and passes without PTO states. For the former, data is mostly distributed horizontally over a wide range of ω_e and a limited range of M_e since moving

Table 7
Summary of tractor use.

Tractor classification	*Time [%]*	*Fuel [%]*	*P_e [kW]*	*ω_e[rpm]*	*$\dot{f}_{sc}$ [g kWh^{-1}]*	*I [%]*
Idling	*25*	*3.6*	*6*	*862*	*338*	*6.3*
Moving	*38*	*36.1*	*43*	*1410*	*229*	*6.2*
Pass without PTO	*16*	*24.0*	*100*	*1701*	*201*	*4.6*
Pass with PTO	*14*	*32.0*	*156*	*1911*	*199*	*3.2*
Headland turn	*7*	*4.3*	*36*	*1593*	*237*	*4.0*

activities were typically low demand and characterised by frequent changes in tractor ground speed. Conversely, for the latter, data is spread vertically over a limited range of ω_e and a wide range of M_e. In comparison, the passes with PTO state occurred in a very narrow operating area, both in terms of ω_e and M_e. This was mostly due to the mechanical constraints of engine-to-PTO transmission and the specific use of the tractor. Indeed, the PTO was mostly operating when the tractor used a power harrow with a width of 5 m, which forced the tractor operator to use the same PTO mode, leading to a small variability in the engine load.

For 26 % of the time when the PTO was engaged, the engine delivered less than 100 kW; in this state, a significant improvement could be obtained by optimising the engine operating point since I might be greater than 5 %. However, for 33 % of the time, P_e was greater than the maximum engine power that could be delivered at the engine speed where the maximum torque is located (i.e. 175 kW), meaning that, in these circumstances, little improvement could be achieved by optimising the engine operating point due to the limited variability of $\dot{f}_{sc}$ along the isopower curves. The tractor operated in 4WD mode for 76 % of the time. Fig. 9 shows the empirical cumulative distributions of P_e when the tractor operated in 2WD and 4WD modes with no use of the PTO. Of particular note is the large difference in P_e between the two operating modes. This occurred because for 90 % of the time when the tractor operated in 2WD mode, it was used for moving tasks, and during these tasks, greater values of P_e occurred only during severe acceleration events [35]. For 80 % of the time, P_e in the 2WD and 4WD modes was below 81 kW and 131 kW, respectively. Comparing these two P_e levels with Fig. 7, the mean value of I at 131 kW is 65 % lower than at 81 kW, indicating that the tractor was much more efficient when operating in 4WD mode than in 2WD mode.

The mean value for annual energy consumption by the tractor was 93.6 MJ. Whilst the tractor was used throughout the year, its use was concentrated in the period between June and October, during which 81.3 % of annual energy was consumed (Fig. 10). This result is due to the typical field management strategy for the fields where the tractor was operating, which are characterised by soils with a high clay content. Under these conditions, farmers typically till fields in autumn – even those dedicated to spring planting – so that they can benefit from soil self-decompaction effects induced by freeze-thaw cycles. Thus, heavy tractors are mostly used in the period between June and October. In June and July, the monitored tractor was mostly used for transportation activities to support combine harvester activities, whilst between August and October, the tractor was mostly used for tillage operations. As shown in Fig. 10, E_e values were particularly large in September and October when fields were tilled before autumn planting, whilst winter soil resting – for spring planting – occurred in March and April.

This seasonality led to a wide distribution of daily E_e, with daily E_e ranging from 65 MJ for very short working days to 3211 MJ for prolonged working days. For 50 % and 95 % of the days, the tractor delivered more than 497 MJ and 2084 MJ, respectively.

3.2. PTO electrification

The 10th and 90th percentile ranges for Δf_{ePTO} with respect P_{ICE} for the passes with PTO is shown in Fig. 11. The lower the P_{ICE}, the greater the range of potential fuel savings due to the greater range of I (Fig. 7), leading to greater opportunities for improved operational efficiency. However, due to the lower efficiency of the ePTO system compared to the mPTO system (Eq. 6 and Eq. 7), Δf_{ePTO} can be negative for any value of P_{ICE}. In particular, the minimum value of Δf_{ePTO} ranged from −3.1 % at 40 kW to −0.1 % at the maximum P_e. This occurred when the engine operated near its optimal point along the isopower curve, at which point the benefits of engine point optimisation did not compensate for the greater power that the engine in the ePTO system had to deliver. This effect was particularly evident at low values of P_{ICE} (lower than 70 kW). Moreover, when the engine operated at points that were far from optimal, Δf_{ePTO} could range from 16 % at 40 kW to 1.8 % at the maximum P_e. This trend decreased for the same reason that I decreased with P_e, as described previously. In Fig. 11, the mean value of Δf_{ePTO} with respect to P_{ICE} is also shown and is above 2 % for P_{ICE} values lower than 90 kW (which occurred for 30 % of the time), whilst at 190 kW, is only 0.8 %.

The potential fuel saving that could be achieved by the study tractor if it was equipped with the ePTO solution was about 1.3 %. This fuel saving is a conservative estimate since the down speed of the engine when the PTO was engaged would also permit a reduction in the power demands of tractor accessories, as they are mechanically driven on agricultural tractors [7]. The fuel saving was low because the tractor was not used for long periods with the PTO operating, and as reported previously, the PTO was mostly used for heavy load applications where the potential for improvements is limited. However, the mean fuel saving could be significantly higher for tractors experiencing prolonged PTO use with low engine loads.

3.3. Plug-in P4 architecture

In Fig. 12, the daily time contribution of each operating mode is reported. The full-electric mode and full ICE mode are the main contributors in terms of time, and both are correlated with battery capacity since they are strictly linked with *SoC* values. For 50 % of the days, the tractor was run on full-electric mode for around 55 % of the time, which occurred on very short and low demand working days. Thus, most of the energy supplied by the battery was supplied from the electricity grid rather than from the tractor's fuel. This is beneficial for the environment because a significant proportion of the Italian electricity mix is generated from renewable energy sources and so the electricity consumed has a lower CO_2 emissions factor than that of diesel fuel [36]. Indeed, the emissions factor for electricity in Italy is two to three times lower than that of a diesel ICE (where the specific fuel consumption of ICE is between 200 and 400 g kWh^{-1}).

Use of the hybrid parallel mode was limited since it only occurred when the operation was classified as high demand, and based on the real-world data, P_e was above $P_{ICE,opt}$ (i.e. 150 kW) for only 13 % of the time when in 4WD mode (Fig. 9). Of note, hybrid recharging had a daily contribution of up to 2 %, which was because the amount of time falling within the low demand operating mode was low. This was due to the series of energy conversions required (i.e. from mechanical to electrical, from electrical to chemical, and from chemical back to mechanical), meaning that the hybrid recharging mode was only convenient when $\dot{f}_{sc}$ was 1.15 greater than $\dot{f}_{sc,min}$, which occurred for 24 % of the time when PTO was not engaged and the engine was not idling. However, load shifting has proved to be much more efficient in passenger cars due to greater variability in specific fuel consumption in passenger car engines compared to those of non-road mobile machinery [37,38], enabling a greater difference in specific fuel consumption between optimal and suboptimal operating conditions. The tractor was used in hybrid series mode for high demand operations, with the battery in low SoC, for up to 19.7 % of the time; however, for 50 % of these days, the tractor was operating in this state for less than 2 % of the time. This indicates that the ICE could be downsized to increase the engine load and reduce the size of tractor accessories, enabling greater fuel efficiency.

The potential fuel, CO_2, and cost savings of the plug-in P4 architecture during the monitoring period were 13.1 %, 9.5 %, and 7.2 %, respectively. These percentages were equivalent to an annual saving of 457 L of fuel, 881 kg_{CO_2}, and €225, respectively. Evidently, these figures could change if the tractor experienced a different use profile to that outlined in Table 7 and for tractors equipped with a gearbox with a different efficiency to the one used in this study. Indeed, the figures are significantly influenced by several parameters, including engine and transmission operating points, workday duration, and types of

operations. The greatest savings occurred in conditions where most of the energy was supplied by the battery, which occurred on days when the tractor was mostly used for low energy demand operations (Fig. 13); this was on short days where the engine was used for low load operations, which occurred on days with the greatest time spent on moving tasks. Moreover, cost saving was negatively correlated with the daily mean value of P_e because the largest cost savings occurred on full electric mode operating for low demand operations where $\dot{f_{sc}}$ was high. For example, on days where the daily value of E_e was approximately 490 MJ, which occurred for 50 % of the days, the cost savings ranged from 5.6 % to 13.7 %, whilst the daily mean value of P_e was between 25 kW and 75 kW.

A sensitivity analysis was undertaken with respect to battery size (ranging from 8.8 kWh to 44 kWh) and variable energy and fuel costs, which are non-marginal factors due to the recent energy crisis. It was observed that the greater the battery size, the greater the fuel saving since the amount of energy supplied by the electricity grid increased at the expense of fuel consumed; consequently, CO_2 savings increased as well. The fuel saving ranged from 7.3 % for a battery size of 8.8 kWh to 13.1 % for a battery size of 44 kWh. According to these figures, increasing battery size from 8.8 kWh to 44 kWh resulted in an annual saving of €59, equivalent to a cost saving of 1.6 € kWh^{-1} per year. Based on an actual cost of lithium-ion batteries of 139 $ kWh^{-1} [39] (equivalent to 129 € kWh^{-1}), increasing the battery size may be uneconomical for farmers as the battery payback period would be longer than the typical economic life of an agricultural tractor (i.e. 12 years according to ASAE [40]). An increase in battery size increased also the CO_2 savings ranging from 6.2 % to 9.6 %. Based on these values, increasing battery size from 8.8 kWh to 44 kWh would produce a total annual saving of 318 kg_{CO_2}, which would be equivalent to an annual saving of 9.0 $kg_{CO_2}\ kWh^{-1}$. However, as the manufacture of a lithium-ion battery produces an average of 150 $kg_{CO_2}\ kWh^{-1}$ [41], increasing battery size might not be environmentally beneficial since the environmental payback period would extended for more than 12 years for each additional kWh. Despite this, given the expected low carbon electricity transition, this environmental payback period could be reduced by 50 % by 2050 [42] making this solution more environmentally beneficial in the future.

Considering recent global developments that have led to increasing inflation and an increase in fuel and electricity costs, cost savings were calculated using historical trends in electricity and fuel costs, enabling evaluation of the cost savings of the plug-in P4 solution in different energy cost scenarios (Fig. 14). Electricity costs were retrieved from the Eurostat database for the Italian market [31], whilst fuel costs for agricultural purposes were retrieved from the CLAL database [30]. Since 2015, energy costs have significantly increased; for example, fuel was 71 % more expensive in 2022 than in 2015, whilst electricity was 117 % more expensive in 2023 than in 2015. This had an impact on the potential cost savings of the plug-in P4 architecture, which ranged from 3.8 % in 2023 to 8.1 % in 2018, producing an annual saving of €63 and €212, respectively. Since the main benefit of the plug-in P4 architecture is to promote electricity energy use over fossil fuel consumption, the optimal condition for cost savings occurred when fuel costs were high compared to electricity costs. However, in many European Union (EU) countries, fuel tax concessions are granted to farmers [43] and this makes continued fossil fuel use economically advantageous for agriculture.

4. Conclusions

Reduced fuel consumption is a key objective in the development of modern tractors as it leads to reduced environmental emissions, operating costs, and customer satisfaction. Drivetrain electrification is potentially one of the most promising solutions to support this goal, but designing an effective electrified drivetrain is not an insignificant task given the numerous variables spread across different levels.

In this study, operational inefficiencies were identified using real-world tractor use data. This approach enabled the identification of effective electric drivetrain concepts and the analysis of their potential fuel savings under actual farming conditions. The results, although derived from a simplified model, demonstrate significant real-world benefits at the test farm, particularly highlighting the potential for fuel savings. For example, the ePTO architecture shows significant promise for tasks that engage the PTO for extended periods at low demand, such as operating fertilizer spreaders and boom sprayers. These tasks typically require tractors equipped with engines that exceed the necessary power due to mass requirements, not power demands.

In addition to cost savings, the plug-in P4 architecture offer several benefits, such as increasing tractor steerability through a pull-in-turn function, gearbox downsizing, and consequent reduced manufacturing costs. This architecture is also environmentally beneficial, particularly as the proportion of electricity from renewable sources increases (notably, the CO_2 emissions factor for electricity in Italy decreased by 7 % from 2012 to 2017) and it is expected that the figures reported in this paper might increase in the near future.

The methodology and results reported in this paper can be used to identify novel drivetrain concepts and are intended to provide a decision-making tool to support further investigations (i.e. accurate system modelling, component sizing, and construction of prototypes). The solutions reported in this study will support the development of approaches to reduce GHG emissions in the future and help to defossilise agriculture.

Discolure statement

During the preparation of this work the author(s) used [NAME TOOL/SERVICE] in order to [REASON]. After using this tool/service, the author(s) reviewed and edited the content as needed and take(s) full responsibility for the content of the publication.

CRediT authorship contribution statement

Michele Mattetti: Writing – original draft, Formal analysis, Data curation, Conceptualization. **Gianvito Annesi:** Writing – review & editing, Formal analysis, Data curation. **Francesco Pio Intrevado:** Writing – review & editing, Visualization, Validation. **Luigi Alberti:** Writing – review & editing, Visualization, Funding acquisition.

Declaration of competing interest

The authors declare that they have no known competing financial interests or personal relationships that could have appeared to influence the work reported in this paper.

Data availability

Data will be made available on request.

Acknowledgements

The activities reported in this paper were part of the project "*Green SEED: Design of more-electric tractors for a more sustainable agriculture*", which was supported by the Ministry of University and Research (MUR) under the call PRIN (Research projects of significant national interest) notification 2017. Grant number: 2017SW5MRC.

References

[1] European Environment Agency. Climate and energy in the EU 2021. https://climate-energy.eea.europa.eu; 2022. accessed January 5.
[2] Ettl J, Bernhardt H, Pickel P, Remmele E, Thuneke K, Emberger P. Transfer of agricultural work operation profiles to a tractor test stand for exhaust emission

evaluation. Biosyst Eng 2018;176:185–97. https://doi.org/10.1016/j.biosystemseng.2018.10.016.
[3] Scolaro E, Beligoj M, Estevez MP, Alberti L, Renzi M, Mattetti M. Electrification of agricultural machinery: a review. IEEE Access 2021;9:164520–41. https://doi.org/10.1109/ACCESS.2021.3135037.
[4] Moreda GP, Muñoz-García MA, Barreiro P. High voltage electrification of tractor and agricultural machinery – a review. Energy Convers Manag 2016;115:117–31. https://doi.org/10.1016/j.enconman.2016.02.018.
[5] Scarlat N, Dallemand JF, Motola V, Monforti-Ferrario F. Bioenergy production and use in Italy: recent developments, perspectives and potential. Renew Energy 2013;57:448–61. https://doi.org/10.1016/j.renene.2013.01.014.
[6] Mattetti M, Beltramin A, Perez Estevez MA, Varani M, Renzi M, Alberti L. Start and stop systems on agricultural tractors as solution for saving fuel and emissions. Biosyst Eng 2022;216:108–20. https://doi.org/10.1016/j.biosystemseng.2022.02.006.
[7] Saetti M, Mattetti M, Varani M, Lenzini N, Molari G. On the power demands of accessories on an agricultural tractor. Biosyst Eng 2021;206:109–22. https://doi.org/10.1016/j.biosystemseng.2021.03.015.
[8] Varani M, Perez Estevez MA, Renzi M, Alberti L, Mattetti M. Controlling idling: a ready-made solution for reducing exhaust emissions from agricultural tractors. Biosyst Eng 2022;221:283–92. https://doi.org/10.1016/j.biosystemseng.2022.07.011.
[9] Mattarelli E, Rinaldini CA, Scrignoli F, Fregni P, Gaioli S, Franceschini G, et al. Potential of electrification applied to non-road diesel engines. SAE Tech Papers 2019. https://doi.org/10.4271/2019-24-0202. 2019-24–0202.
[10] Fraser N, Blaxill H, Lumsden G, Bassett M. Challenges for increased efficiency through gasoline engine downsizing. SAE Int J Engines 2009;2:991–1008.
[11] Mattetti M, Medici M, Canavari M, Varani M. CANBUS-enabled activity-based costing for leveraging farm management. Comput Electron Agric 2022;194:106792. https://doi.org/10.1016/j.compag.2022.106792.
[12] Thomas RS, Buckmaster DR. Development of a computer-controlled, hydraulic, power take-off (PTO) system. Trans of the ASAE 2005;48:1669–75.
[13] Beligoj M, Scolaro E, Alberti L, Renzi M, Mattetti M. Feasibility evaluation of hybrid electric agricultural tractors based on life cycle cost analysis. IEEE Access 2022;10:28853–67. https://doi.org/10.1109/ACCESS.2022.3157635.
[14] Mocera F, Somà A. Analysis of a parallel hybrid electric tractor for agricultural applications. Energies 2020;13:3055. https://doi.org/10.3390/en13123055.
[15] Varani M, Mattetti M, Molari G. Performance evaluation of electrically driven agricultural implements powered by an external generator. Agronomy 2021;11:1447. https://doi.org/10.3390/agronomy11081447.
[16] Vukovic M, Leifeld R, Murrenhoff H. Reducing fuel consumption in hydraulic excavators—a comprehensive analysis. Energies 2017;10:687. https://doi.org/10.3390/en10050687.
[17] Angelucci L, Mattetti M. The development of reference working cycles for agricultural tractors. Biosyst Eng 2024;242:29–37. https://doi.org/10.1016/j.biosystemseng.2024.04.004.
[18] Lee B, Lee S, Cherry J, Neam A, Sanchez J, Nam E. Development of advanced light-duty powertrain and hybrid analysis tool. Warrendale, PA: SAE International; 2013. https://doi.org/10.4271/2013-01-0808.
[19] SAE. SAE J1939–14 - Physical Layer, 500 Kbps. 2016.
[20] SAE. SAE J1939–15 - Physical Layer, 250 Kbps. 2018.
[21] Esteban B, Riba J-R, Baquero G, Rius A, Puig R. Temperature dependence of density and viscosity of vegetable oils. Biomass Bioenergy 2012;42:164–71. https://doi.org/10.1016/j.biombioe.2012.03.007.
[22] OECD. OECD code 2 report - New Holland T7.260. Weiselburg (AT). 2011.
[23] Mattetti M, Maraldi M, Lenzini N, Fiorati S, Sereni E, Molari G. Outlining the mission profile of agricultural tractors through CAN-BUS data analytics. Comput Electron Agric 2021;184:106078. https://doi.org/10.1016/j.compag.2021.106078.
[24] Mattetti M, Maraldi M, Sedoni E, Molari G. Optimal criteria for durability test of stepped transmissions of agricultural tractors. Biosyst Eng 2019;178:145–55. https://doi.org/10.1016/j.biosystemseng.2018.11.014.
[25] Alberti L, Troncon D. Design of Electric Motors and Power Drive Systems According to efficiency standards. IEEE Trans Ind Electron 2021;68:9287–96. https://doi.org/10.1109/TIE.2020.3020028.
[26] Gu Y, Kushwaha RL. Dynamic load distribution and tractive performance of a model tractor. J Terrramech 1994;31:21–39. https://doi.org/10.1016/0022-4898(94)90030-2.
[27] Markel T, Simpson A. Cost-benefit analysis of plug-in hybrid electric vehicle technology. World Electric Vehicle J 2007:1. https://doi.org/10.3390/wevj1010294.
[28] Pettersson K. Design automation of complex Hydromechanical transmissions. 2013.
[29] Manzetti S, Mariasiu F. Electric vehicle battery technologies: from present state to future systems. Renew Sust Energ Rev 2015;51:1004–12. https://doi.org/10.1016/j.rser.2015.07.010.
[30] CLAL. TESEO: cost of fuel for agricultural use 2024. https://teseo.clal.it/?section=gasolio_agricolo; 2024. accessed January 28.
[31] Eurostat. Electricity prices for household consumers - bi-annual data (from 2007 onwards) 2024. https://ec.europa.eu/eurostat/databrowser/view/nrg_pc_204/default/table?lang=en; 2024. accessed January 16.
[32] Geerlings H, van Duin R. A new method for assessing CO2-emissions from container terminals: a promising approach applied in Rotterdam. J Clean Prod 2011;19:657–66. https://doi.org/10.1016/j.jclepro.2010.10.012.
[33] Climate Transparency. Climate Transparency, 2019. Brown to Green - The G20 Transition Towards a Net-Zero Emissions Economy. 2019.
[34] Mattetti M, Varani M, Maraldi M, Paolini F, Fiorati S, Molari G. Tractive performance of Trelleborg PneuTrac tyres. J Agri Eng 2020;51:100–6. https://doi.org/10.4081/jae.2020.1031.
[35] Mattetti M, Michielan E, Mantovani G, Varani M. Objective evaluation of gearshift process of agricultural tractors. Biosyst Eng 2022;224:324–35. https://doi.org/10.1016/j.biosystemseng.2022.11.001.
[36] Noussan M, Roberto R, Nastasi B. Performance indicators of electricity generation at country level—the case of Italy. Energies 2018;11:650. https://doi.org/10.3390/en11030650.
[37] Legg T, Nelson D. Development of a Willans line rule-based hybrid energy management strategy. Warrendale, PA: SAE International; 2022. https://doi.org/10.4271/2022-01-0735.
[38] Sarioglu İL, Klein OP, Schroder H, Kucukay F. Energy Management for Fuel-Cell Hybrid Vehicles Based on specific fuel consumption due to load shifting. IEEE Trans Intell Transp Syst 2012;13:1772–81. https://doi.org/10.1109/TITS.2012.2204878.
[39] BloombergNEF. Lithium-Ion Battery Pack Prices Hit Record Low of $139/kWh | BloombergNEF 2023. https://about.bnef.com/blog/lithium-ion-battery-pack-prices-hit-record-low-of-139-kwh/; 2024. accessed January 28.
[40] ASAE. ASAE D497.7 - Agricultural Machinery Management Data. 2015.
[41] Bouter A, Guichet X. The greenhouse gas emissions of automotive lithium-ion batteries: a statistical review of life cycle assessment studies. J Clean Prod 2022;344:130994. https://doi.org/10.1016/j.jclepro.2022.130994.
[42] Xu C, Steubing B, Hu M, Harpprecht C, van der Meide M, Tukker A. Future greenhouse gas emissions of automotive lithium-ion battery cell production. Resour Conserv Recycl 2022;187:106606. https://doi.org/10.1016/j.resconrec.2022.106606.
[43] OECD. OECD Companion to the Inventory of Support Measures for Fossil Fuels 2018. 2018.